Side Chain Dispersity Matters: Topologically Precise and Discrete Bottlebrush Polymers

Nduka D. Ogbonna, † Michael Dearman, † Cheng-Ta Cho, † Bhuvnesh Bharti, † Andrew J. Peters, ‡ Jimmy Lawrence. †,*

†Department of Chemical Engineering, Louisiana State University, Baton Rouge, 70803, United States.

‡Department of Chemistry, Louisiana State University, Baton Rouge, 70803, United States.

KEYWORDS: polymerization kinetics, precision bottlebrush polymers, Langmuir-Blodgett, glass transition temperature, discrete macromonomer, discrete bottlebrushes.

ABSTRACT: The synthesis of bottlebrush polymers with topologically precise and fully discrete structures is reported. Key features of the synthesis include the combination of scalable synthesis and separation strategies to access discrete macromonomer libraries, followed by their polymerization and further separation into topologically uniform and discrete bottlebrushes. Discrete macromonomer proves crucial for regulating the structural heterogeneity of bottlebrushes and their macroscopic properties. When assembled as a monolayer at the air-water interface, bottlebrushes with discrete side chains display high packing density and distinct three-phase Langmuir-Blodgett isotherms. The impact of precisely regulating side chain dispersity and sequence on polymer properties was further demonstrated through tailoring the interbrush interactions and thermomechanical properties of well-defined block bottlebrushes.

INTRODUCTION

As the complexity of polymer structure grows, so do the challenges for developing fundamental understanding of their structure-property relationships. Branched polymers such as bottlebrush polymers (BBP, **Scheme 1a**) are promising material platforms for ultra-soft interfaces, sensing, and delivery applications[1–6] because they possess unique entanglement-free rheology and high functional group density.[7–9] In the past decade, the synthesis of complex BBPs with myriad polymeric side chain architectures has been enabled by the development of *grafting-to, -from,* and *-through* strategies.[10–13] However, such multifunctional BBPs have disperse backbone and side chains, and thus, their properties reflect a broad distribution of species, not the individual brushes. Each layer of dispersity introduced in the BBP synthesis amplifies the number of species in the mixture in an exponential manner (**Scheme 1b**). This challenge is further compounded by limitations for estimating BBP structure. For BBPs prepared by *grafting-through*, the backbone degree of polymerization (N_{BB}) is calculated by dividing its averaged total molecular weight (M_n) from light scattering analysis by the M_n of the disperse macromonomer. Given the side chain length is not identical across the backbone length of BBP,[14–16] understanding the impact of structural precision on BBP heterogeneity and properties remains a grand challenge.

Scheme 1. Synthesis of topologically uniform, discrete, and block bottlebrush polymers (*Đ:* dispersity index, N_{BB}: backbone degree of polymerization, N_{SC}: side chain degree of polymerization).

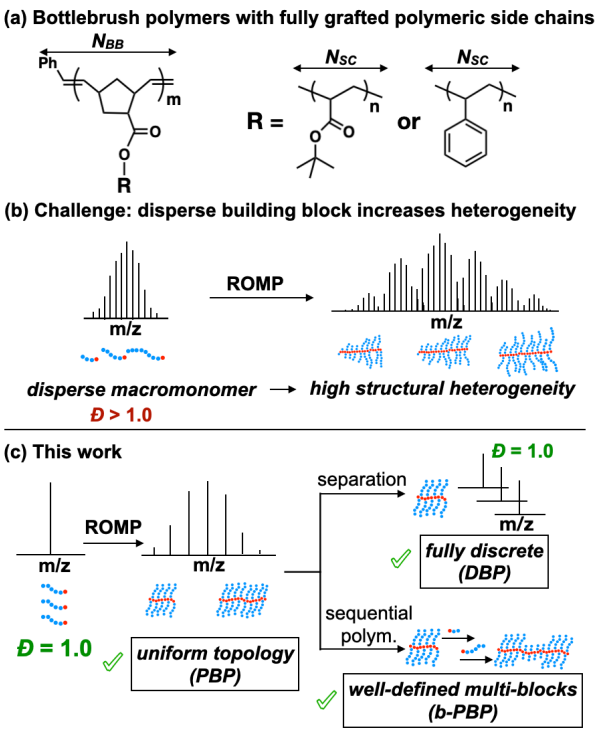

Understanding the structure-property relationship of bottlebrush polymers is crucial for their rational design. Inspired by the well-defined structure and functional precision of aggrecan,[17,18] a bottlebrush-like biopolymer, we synthesized a library of topologically uniform ('truly cylindrical'[19]) precision bottlebrush polymers (**PBP,** $Đ_{SC}$ = 1.0) using discrete macromonomers (**Scheme 1c**). Previous studies have shown that discrete oligomers and polymers exhibit strong length-dependent properties distinct from their disperse counterparts.[20–27] Without controlling side chain dispersity, the permutation of side chain arrangements in conventional BBPs imposes a significant challenge for understanding their structure-property relationships, especially at the underexplored regime of low N_{BB} and N_{SC}.[28–30]

Here we report both the properties and topology of BBPs are significantly impacted by the dispersity of their side chains. To date, only grafting-through techniques such as ring-opening metathesis polymerization (ROMP) can yield BBPs with fully grafted polymeric/bulky side chains.[31–33] However, the rapid kinetics of ROMP can lead to the assumption that all macromonomer species polymerize at a similar rate. Contrary to this assumption, we found the rate of grafting-through ROMP is impacted by macromonomer size, especially at $N_{SC} < 10$, where the impact of dispersity is more pronounced. The significant polymerization rate difference between macromonomer species in disperse mixtures raises the concern of topological accuracy and structural heterogeneity in disperse BBPs. The polymerization of discrete macromonomers described in this study addresses this challenge because it yields bottlebrushes with uniform and tailorable side chain topology. Importantly, the well-defined structure of PBPs opens access to truly discrete bottlebrush polymers (**DBP**, $Đ_{BB}$ & $Đ_{SC}$ = 1.0**)**. As we show later, a scalable strategy to prepare a range of PBPs in linear and block topology enables us to examine the impact of side chain dispersity on the physical and thermomechanical properties of brush polymers. The broad scope of this strategy was also illustrated through the synthesis of acrylate- and styrenic-bottlebrushes.

RESULTS AND DISCUSSION

Synthesis of macromonomers and bottlebrush polymers. Macromonomer libraries were prepared through a combination of controlled polymerization, post-functionalization, and separation strategies (see Supporting Information).[22,27,28,34–38] This multi-step approach is critical for removing traces of nonfunctional byproducts and impurities.[39] Vinyl monomers were chosen for this study because of their wide monomer scope, synthetic versatility, and potential relevance toward other bulky macromonomers (*e.g.*, branched alkyl, conjugated).[40] A polymeric side chain of $N_{SC} \approx 10$ is comparable to C20 alkyl side chain lengthwise.

All macromonomers and bottlebrush polymers synthesized in this study were characterized using NMR, size-exclusion chromatography (SEC), and MALDI-ToF (**Table SI-1**). As an example, ^{1}H NMR analysis confirmed the quantitative conversion of tetrameric bromine terminated oligo(*tert*-butyl acrylate) (oTBA4-Br) into norbornenyl-oTBA4 discrete macromonomers (**T4**), as seen in the downfield shift of the chain-end methine protons from 4.1 to 4.8 ppm and the appearance of the norbornenyl cyclic alkene proton at 6.1 ppm. Ideal integration ratios were seen for all characteristic peaks of discrete macromonomers (**Figure S3-5**). The structural purity of discrete macromonomers was confirmed using SEC and MALDI-ToF (single molecular peak, calculated for **T4** = 664.42, observed = 664.45, **Figure S22-23**).

With disperse and discrete macromonomers in hand, bottlebrush polymers with tailored N_{BB} and N_{SC} were synthesized using pyridine-ligated Grubbs 3rd generation catalyst (G3). G3 catalyst is well-suited for kinetic studies as initial screening confirmed its slower polymerization rate relative to other G3 variants (~20% of 3-bromopyridine-ligated G3), in agreement with literature.[41] The averaged total molecular weight of BBPs and PBPs were estimated using SEC equipped with multi-angle light scattering detector, and the molecular mass of unimolecular DBPs was determined using MALDI-ToF. A stochastic model was constructed to simulate the molecular weight distributions of the BBP and the distribution of side chains along the backbone (see Supporting Information).

The impact of macromonomer dispersity on polymerization kinetics. Through examining the *grafting-through* ROMP kinetics of disperse and discrete macromonomers, we found the propagation rate constant (k_p) of short macromonomers ($N_{SC} < 10$) to be inversely proportional to the square root of their chain length. While length-dependent propagation rate behavior was recently observed for disperse macromonomers with N_{SC} up to 50,[42] we hypothesized that the pronounced impact of dispersity, especially on short polymer chains, will necessitate the use of discrete systems to obtain accurate and reproducible k_p values. Following standard procedures, macromonomer conversion was calculated by analyzing the NMR spectra (olefin protons of terminal norbornene at 6.1 ppm) and SEC traces[36,43] of aliquots taken during the polymerization of macromonomers. Deconvoluting the SEC signal of disperse system using a Gaussian fitting algorithm suggested that within 30 s, the trimer macromonomer is consumed ~25% faster than the pentameric species (**Figure 1b**). This finding attracted our attention because the propagation kinetics of norbornenyl macromonomers under ROMP condition is fast and less sterically hindered, and therefore the controlled chain growth process with increasing macromonomer conversion is often attributed to similar macromonomer reactivity.[44]

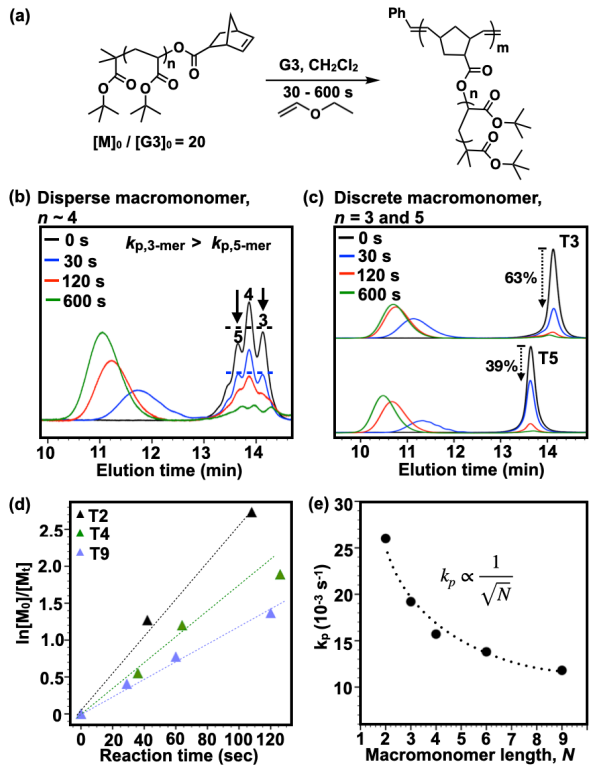

Figure 1. (a) Bottlebrush polymer synthesis via grafting-through ROMP. (b) SEC RI traces of ROMP of disperse tetramer, **NB-otBA$_4$** at various reaction times. (c) SEC traces of ROMP of discrete trimer, **T3** and pentamer, **T5**. (d) $\ln[M_0]/[M]_t$ vs polymerization time for discrete macromonomers. (e) k_p vs length of the discrete macromonomers, T2–T9. The total peak areas of all SEC traces were normalized to unity.

To obtain accurate propagation rate constants, we synthesized a library of discrete macromonomers (dimer to nonamer, **T2–T9**) and examined their homopolymerization kinetics. The trimeric T3 polymerizes 50% faster than the pentameric T5 (**Figure 1c**), and the propagation rate of T2 is ~220% the rate of T9 ($k_{p,T2}$ = 26 × 10^{-3} s^{-1}, $k_{p,T9}$ = 11.8 × 10^{-3} s^{-1}, **Figure 1d**). The polymerization of each discrete macromonomer maintains its living characteristics, as seen in their pseudo-first-order kinetics and the linear relationship between $\ln[M]_0/[M]_t$ and polymerization time (**Figure 1d**). Our kinetic analysis suggests that the polymerization rate of discrete TBA macromonomer ($N < 10$) follows a size-dependent exponential decay with $k_p \sim 1/\sqrt{N}$ (**Figure 1e**).

Importantly, further analysis shows that macromonomer dispersity and size-dependent kinetics significantly amplify the heterogeneity of conventional BBPs, because the propagating brush ends encounter different ratios of shorter and longer macromonomers over time. MALDI-ToF analysis of **BBP-oTBA4$_6$** reveals a multimodal distribution of > 70 bottlebrush species, despite the low dispersity as measured by SEC analysis ($Đ$ = 1.2) (**Figure 2a**). In contrast, the MALDI-ToF spectra of **PBP-T4$_6$** shows a monomodal distribution of only seven species, a decrease of one magnitude in sample heterogeneity. To understand the impact of macromonomer dispersity and size-dependent polymerization rate on heterogeneity, we constructed a stochastic polymerization model using the k_p values for each discrete macromonomer. Accurate and precise input parameters enable the model to reproduce the multimodal heterogeneity observed for BBP sample (**Figure S47**). The model shows that the propagating brush ends encounter an increasing hexamer-to-trimer ratio throughout the polymerization (**Figure S48**), including a recent study by Zhu and coworkers, yield two important insights: (a) conventional BBPs have tapered or asymmetric side chain arrangements and (b) the overall heterogeneity of disperse BBP is significantly impacted by macromonomer composition/dispersity.

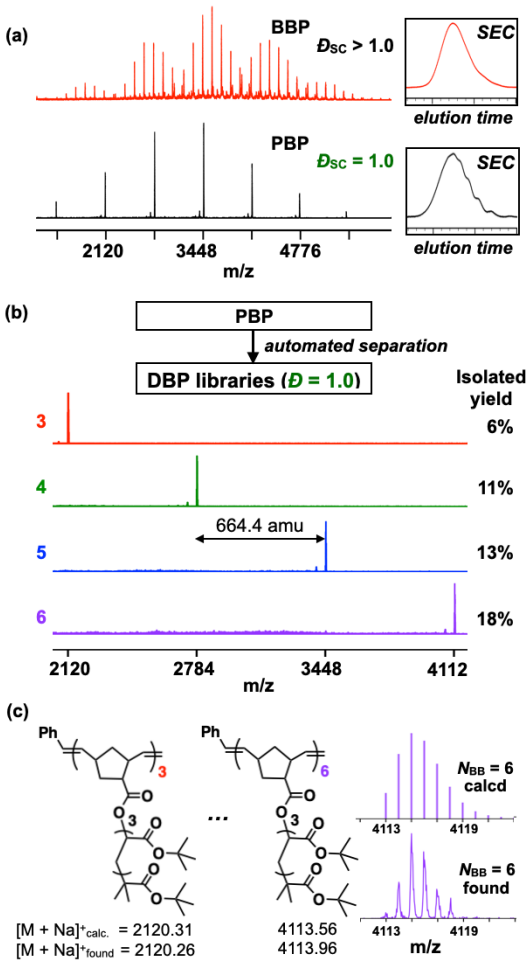

Figure 2. (a) MALDI-ToF spectra and SEC traces of bottlebrush polymers prepared from *grafting-through* ROMP of disperse tetramer (red) and discrete tetramer (black). (b) MALDI-ToF spectra of discrete bottlebrush polymers (**DBP-T4$_n$**) (c) m/z values of DBPs and isotopic distribution analysis of **DBP-T4$_6$**.

Discrete bottlebrush polymers. To fully understand the impact of heterogeneity on the properties of brush polymers and advance future simulation models,

access to truly discrete bottlebrushes ($Đ$ = 1.0) is desirable. The well-defined composition of PBPs enabled the isolation of fully discrete bottlebrush polymers (**DBP**), with single molecular ions observed by MALDI-ToF analysis correlating to each expected structure. We were initially encouraged by the unique SEC profile of **PBP-T4$_6$**, which shows multiple peaks corresponding to bottlebrushes separated by precisely one tetramer side chain, despite having a similar overall dispersity with **BBP-oTBA4** according to SEC analysis (**Figure 2a**, see also **Figure S31** for other PBP samples). The clear identification of each PBP species proves useful for optimizing the isolation of a library of **DBPs** in a scalable and consistent manner using recycling preparative SEC (**Figure 2b**). NMR, SEC, and MALDI-ToF analysis confirmed the isolation of unimolecular brush polymer libraries in near-quantitative yield. The single molecular ion of **DBP-T4$_6$** corresponds to the sodium adduct of a bottlebrush polymer with precisely 24 *t*-butyl acrylate functional groups (calculated = 4113.56, observed = 4113.96, **Figure 2c**). Having homogeneously distributed functional groups and tailorable three-dimensional structures (N_{BB}/N_{SC} ratio), DBP is a new promising addition to the family of precision macromolecules for targeted and precision technologies.

The impact of dispersity on inter-brush interactions and properties. A question remains regarding the impact of side chain and backbone dispersity and their effect on the properties of bottlebrush polymers. Using a previously established method,[28,45] we constricted inter-brush interactions to a two-dimensional Langmuir-Blodgett (L-B) monolayer and examined three samples, **BBP-oTBA4$_6$** ($Đ_{SC}$ = 1.1), **PBP-T4$_6$** ($Đ_{SC}$ = 1.0,) and **DBP-T4$_6$** ($Đ_{overall}$ = 1.0). Even for a short N_{BB} of 6, only samples with discrete side chains (PBP and DBP) exhibit previously unseen[45–48] sharp liquid-to-solid phase transition. Notably, the packing density of brush polymers at the air-water interface increases significantly as the structure becomes fully discrete (**Figure 3a**). Indeed, the impact of dispersity is important for brush polymers, especially for low N_{SC} and N_{BB}.

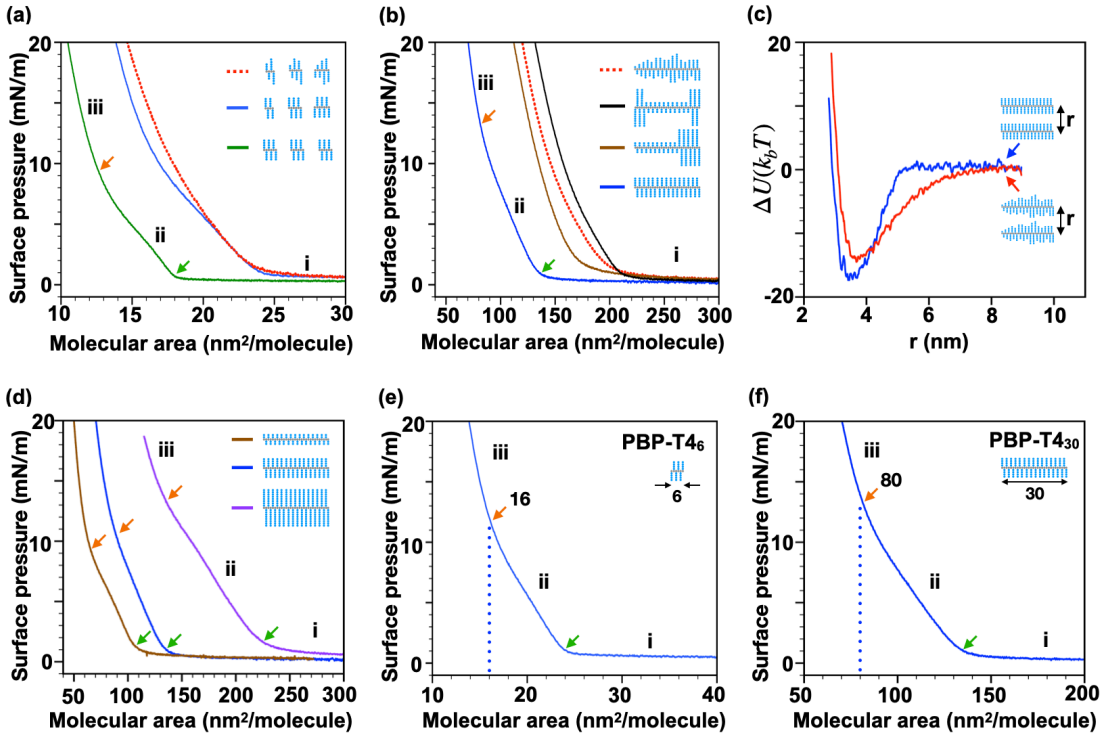

Figure 3. (a) Langmuir-Blodgett (L-B) surface pressure-area isotherms of bottlebrush polymer, **BBP-otBA4$_6$** (red), precision bottlebrush polymer, **PBP-T4$_6$** (blue), and discrete bottlebrush polymer, **DBP-T4$_6$** (green). (b) L-B isotherms of structurally different isomers with $N_{SC} \approx 4$ and $N_{BB} \approx 30$; **BBP-otBA4$_{30}$** (dashed red), **PBP-T4$_{30}$** (blue), **b-PBP-T2$_{20}$T8$_{10}$** (brown), and **b-PBP-T8$_5$T2$_{20}$T8$_5$** (black). (c) Interaction potential energy as a function of backbone distance between parallel bottlebrushes, calculated for samples having disperse (**BBP-otBA4$_{30}$**, red) and discrete (**PBP-T4$_{30}$**, blue) side chains. (d) L-B isotherms of PBPs with $N_{BB} \approx 30$ with different discrete side chain length, **PBP-T2$_{30}$** (brown), **PBP-T4$_{30}$** (blue), and **PBP-T8$_{30}$** (purple). L-B isotherms of topologically uniform (e) **PBP-T4$_6$** and (f) **PBP-T4$_{30}$** with phase transition to close-packed structures labeled. Phase transitions from regime i to ii (gas-to-liquid phase) and ii to iii (liquid-to-solid phase) were determined by taking the first derivative of the isotherms and are indicated with green and orange arrows, respectively. Schematics of bottlebrushes are indicated in the plot legends for clarity.

Interestingly, the distinct first-order phase transitions from gas-to-liquid and especially liquid-to-solid regimes are also observed for larger PBPs. All PBP samples exhibit this unique behavior regardless of their side chain (N_{SC} = 2 to 8) and average backbone length (N_{BB} ≈ 6 to 30) (**Figure 3b**, **d**). In contrast, all disperse side chain samples do not display sharp phase transition from liquid-to-solid regime, presumably due to side chain dispersity-induced topological defects. We speculate that the uniform topology of PBPs imparts homogeneous backbone stiffness and inter-brush interactions. To understand the impact of side chain interactions on packing behavior, brush-brush pair potentials were calculated for coarse-grained models of bottlebrushes with disperse and discrete side chains (BBP and PBP, N_{BB} ≈ 30, N_{SC} ≈ 4). As expected, the disperse side chains of BBP pair interact first at a brush-brush distance of 8 nm gradually, while the side chain-side chain interactions of PBP pair starts at a much shorter distance of 5 nm, followed by a steep potential change to a minimum potential at ~ 3.8 nm (**Figure 3c, Figure S49**). The uniform rigid rod-like behavior of PBP samples and their higher packing density were also confirmed through coarse-grained molecular dynamics studies (Langmuir-Blodgett simulations, **Figure S50**).

Notably, PBP samples display packing behavior that scales proportionately with their side chain length (**Figure S41**), which confirms their uniform backbone stiffness and rod-like behavior upon compression at the air-water interface (**Figure 3d**). Owing to their discrete side chains, the phase transition point from liquid-to-solid for **PBP-T4$_{30}$** is precisely 5 times that of **PBP-T4$_6$** (80 vs 16 nm^2/molecule, **Figure 3e-f** and **Figure S42**). Collectively, our results highlight the first observation of both early interactions between bottlebrushes (gas-to-liquid) and the eventual side chain-side chain interaction upon compression (liquid-to-solid), with the overall packing efficiency being strongly impacted by topological uniformity.

Designing side chain topology to tailor functions. The spatial feature of polymers determines their conformational and thermomechanical properties. To illustrate the importance of macromonomer dispersity and designer topology, three architectural variants/isomers were prepared via sequential block polymerization: **PBP-T4$_{30}$** (homo-T4), **b-PBP-T2$_{20}$T8$_{10}$** (diblock-T2/8), and b-PBP-T8$_5$T2$_{20}$T8$_5$ (triblock-T8/2/8) (**Figure 4a, S12-15,32-33**). Encouragingly, the block size in these b-PBP samples could be estimated using NMR analysis (**Figure 4a**). L-B studies of these variants clearly demonstrate that a slight change in side chain topology dramatically affects the interbrush interactions of bottlebrush polymers (**Figure 3b, S40**). Among bottlebrush samples with average N_{SC} ≈ 4, the surface pressure (Π) increase is observed first for the triblock at 210 molecule/nm^2, followed by the diblock (170 molecule/nm^2), and linear brush (135 molecule/nm^2). The significantly lower packing efficiency of the triblock brushes is attributed to the presence of octamer blocks at both brush ends, which increase voids between dimer sections, as also confirmed via coarse-grained MD simulations (**Figure S51**). Furthermore, the onset of Π increase for the triblock-T8/2/8 sample at 210 molecule/nm^2 (**Figure 3b**) is comparable to the onset of Π increase for PBP with octamer side chains (**PBP-T8$_{30}$**, 225 molecule/nm^2, **Figure 3d, S40**), which suggests that homo- and multiblock PBPs can be designed to assemble into monolayers with tailorable void space (**Figure S50, 51**).

Importantly, the dispersity and block sequence of side chains have a significant impact on the thermomechanical properties of bottlebrush polymers. To study the impact of side chain topology on glass transition temperatures (T_g), we prepared three poly(styrene)-based bottlebrush variants/isomers, all of which are glassy solid at ambient temperature (**Figure 4b**): disperse **BBP-S4$_{30}$** (disperse-S4, control), **PBP-S4$_{30}$** (homo-S4), and **b-PBP-S2$_{20}$S8$_{10}$** (diblock-S2/8). Differential scanning calorimetry (DSC) analysis shows that the disperse-S4 sample has a T_g of 31 °C. To our surprise, the **PBP-S4$_{30}$** sample exhibits a significantly higher T_g of 46 °C, a difference of 15 °C by simply making the side chain discrete **(Figure 4c**). Such a difference can be explained by assuming that side chain dispersity increases free-volume, as indicated by L-B studies described above. The higher packing efficiency of the PBP sample observed in L-B studies was also confirmed by DSC analysis, as the first scan of PBP and diblock-PBP display small enthalpy relaxation peaks commonly seen in polymers undergoing molecular relaxation/densification (**Figure S45**). Notably, while the diblock-S2/8 sample has a lower M_n and larger free volume than the homobrush PBP-S4$_{30}$, it exhibits a higher T_g of ≈ 50 °C. This result suggests the minor octamer block plays a more significant role in affecting bottlebrush T_g than the major dimer block. Overall, the striking T_g difference between conventional disperse BBP and diblock PBP (ΔT_g ≈ 20 °C) underlines the importance of topological design and its versatility for tuning thermomechanical properties.

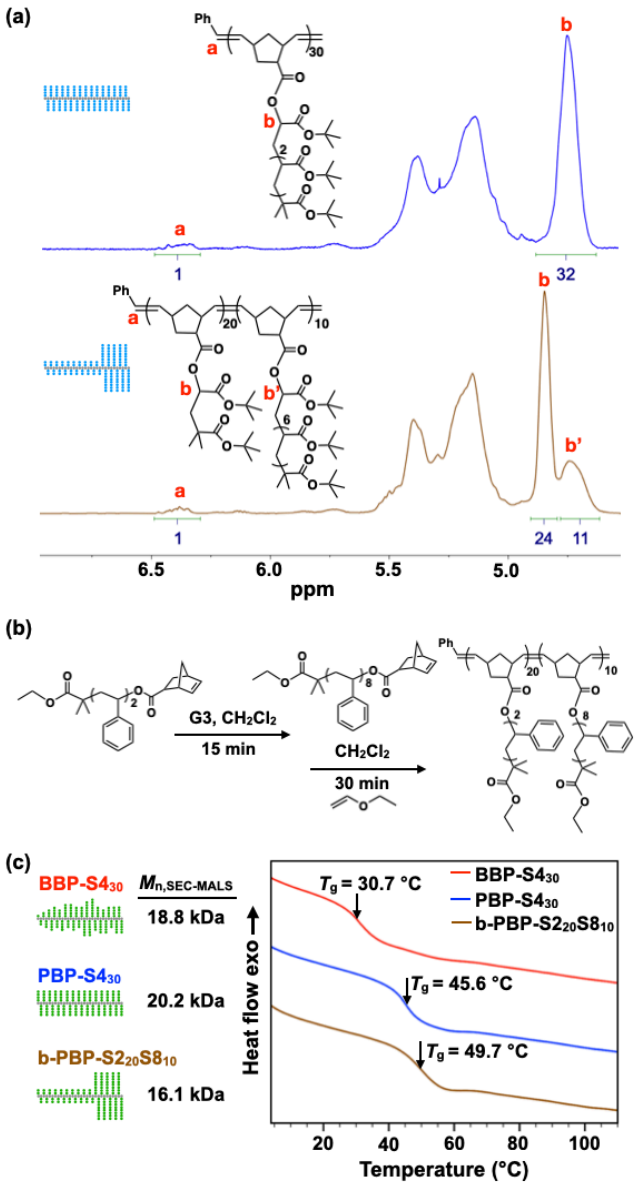

Figure 4. (a) ^{1}H NMR spectra of homobrush **PBP-T4$_{30}$** (blue) and diblock **PBP-T2$_{20}$T8$_{10}$** (brown). (b) Synthesis of styrenic b-PBP (c) DSC traces of disperse **BBP-S4$_{30}$** (red), homobrush **PBP-S4$_{30}$** (blue), and diblock **b-PBP-S2$_{20}$S8$_{10}$** (brown).

CONCLUSION

In summary, we describe the synthesis of topologically precise and discrete bottlebrush polymer libraries, and highlight the importance of side chain dispersity. Our kinetic studies support our hypothesis that macromonomer size and dispersity have a substantial impact on polymerization kinetics which affects the topology of bottlebrush polymers. Our scalable and efficient strategy to prepare bottlebrush polymers with uniform and tailored topology represents a powerful approach for tuning their physical and thermomechanical properties. The significant potential of side chain dispersity and topology design is illustrated in striking differences in monolayer phase transitions, packing efficiency, and glass transition temperatures between bottlebrushes having disperse and discrete side chains. New fundamental insights and precision models are indeed crucial for enabling a closer integration between experimental and theoretical studies, especially for designing complex soft materials with small three-dimensional features and precise functions, as we have demonstrated through the first report of topologically precise and fully discrete bottlebrush polymers.

ASSOCIATED CONTENT

Supporting Information

The Supporting Information is available from the ChemRxiv server.

Experimental procedures and characterization data (NMR, MALDI-ToF, SEC, FTIR, LB) for all samples (PDF)

AUTHOR INFORMATION

Corresponding Author

Jimmy Lawrence — Department of Chemical Engineering, Louisiana State University, Baton Rouge, 70803, United States; https://orcid.org/0000-0003-4455-6177; Email: jimmylawrence@lsu.edu

The manuscript was written through contributions of all authors. All authors have given approval to the final version of the manuscript. The authors declare no competing financial interest.

ACKNOWLEDGMENT

N.O. and J.L. acknowledge the support from Louisiana Board of Regents funding (RD-A-07), the American Chemical Society Petroleum Research Fund (62656-DN17), and BASF Living Sustainability Laboratory Program. B.B. acknowledges the support from NSF-CAREER (CBET-1943986). A. J. P. acknowledges Louisiana Board of Regents funding (RD-A-18). The authors acknowledge the support for material characterizations by the NMR, Polymer Analysis Laboratory (Dr. Rafael Cueto), and Shared Instrumentation Facilities at Louisiana State University (Dr. Fabrizio Donnarumma). The high-performance computing resources provided by the Louisiana Optical Network Infrastructure (https://loni.org) were used for this work.

REFERENCES

(1) Keith, A. N.; Vatankhah-Varnosfaderani, M.; Clair, C.; Fahimipour, F.; Dashtimoghadam, E.; Lallam, A.; Sztucki, M.; Ivanov, D. A.; Liang, H.; Dobrynin, A. V.; Sheiko, S. S. Bottlebrush Bridge between Soft Gels and Firm Tissues. *ACS Cent Sci* **2020**, *6* (3), 413–419.

(2) Reynolds, V. G.; Mukherjee, S.; Xie, R.; Levi, A. E.; Atassi, A.; Uchiyama, T.; Wang, H.; Chabinyc, M.

L.; Bates, C. M. Super-Soft Solvent-Free Bottlebrush Elastomers for Touch Sensing. *Mater. Horiz.* **2020**, *7* (1), 181–187.

(3) Mukumoto, K.; Averick, S. E.; Park, S.; Nese, A.; Mpoukouvalas, A.; Zeng, Y.; Koynov, K.; Leduc, P. R.; Matyjaszewski, K. Phototunable Supersoft Elastomers Using Coumarin Functionalized Molecular Bottlebrushes for Cell-Surface Interactions Study. *Macromolecules* **2014**, *47* (22), 7852–7857.

(4) Xu, H.; Sun, F. C.; Shirvanyants, D. G.; Rubinstein, M.; Shabratov, D.; Beers, K. L.; Matyjaszewski, K.; Sheiko, S. S. Molecular Pressure Sensors. *Adv. Mater.* **2007**, *19* (19), 2930–2934.

(5) Johnson, J. A.; Lu, Y. Y.; Burts, A. O.; Lim, Y.-H.; Finn, M. G.; Koberstein, J. T.; Turro, N. J.; Tirrell, D. A.; Grubbs, R. H. Core-Clickable PEG-Branch-Azide Bivalent-Bottle-Brush Polymers by ROMP: Grafting-through and Clicking-To. *J. Am. Chem. Soc.* **2011**, *133* (3), 559–566.

(6) Yu, Y.; Chen, C.-K.; Law, W.-C.; Mok, J.; Zou, J.; Prasad, P. N.; Cheng, C. Well-Defined Degradable Brush Polymer–Drug Conjugates for Sustained Delivery of Paclitaxel. *Mol. Pharm.* **2013**, *10* (3), 867–874.

(7) Sheiko, S. S.; Sumerlin, B. S.; Matyjaszewski, K. Cylindrical Molecular Brushes: Synthesis, Characterization, and Properties. *Prog. Polym. Sci.* **2008**, *33* (7), 759–785.

(8) Namba, S.; Tsukahara, Y.; Kaeriyama, K.; Okamoto, K.; Takahashi, M. Bulk Properties of Multibranched Polystyrenes from Polystyrene Macromonomers: Rheological Behavior I. *Polymer* **2000**, *41* (14), 5165–5171.

(9) Wintermantel, M.; Gerle, M.; Fischer, K.; Schmidt, M.; Wataoka, I.; Urakawa, H.; Kajiwara, K.; Tsukahara, Y. Molecular Bottlebrushes. *Macromolecules* **1996**, *29* (3), 978–983.

(10) Gao, H.; Matyjaszewski, K. Synthesis of Molecular Brushes by "Grafting Onto" Method: Combination of ATRP and Click Reactions. *J. Am. Chem. Soc.* **2007**, *129* (20), 6633–6639.

(11) Beers, K. L.; Gaynor, S. G.; Matyjaszewski, K.; Sheiko, S. S.; Möller, M. The Synthesis of Densely Grafted Copolymers by Atom Transfer Radical Polymerization. *Macromolecules* **1998**, *31* (26), 9413–9415.

(12) Xia, Y.; Kornfield, J. A.; Grubbs, R. H. Efficient Synthesis of Narrowly Dispersed Brush Polymers via Living Ring-Opening Metathesis Polymerization of Macromonomers. *Macromolecules* **2009**, *42* (11), 3761–3766.

(13) Walsh, D. J.; Dutta, S.; Sing, C. E.; Guironnet, D. Engineering of Molecular Geometry in Bottlebrush Polymers. *Macromolecules* **2019**, *52* (13), 4847–4857.

(14) Rathgeber, S.; Pakula, T.; Wilk, A.; Matyjaszewski, K.; Beers, K. L. On the Shape of Bottle-Brush Macromolecules: Systematic Variation of Architectural Parameters. *J. Chem. Phys.* **2005**, *122* (12), 124904.

(15) Dutta, S.; Wade, M. A.; Walsh, D. J.; Guironnet, D.; Rogers, S. A.; Sing, C. E. Dilute Solution Structure of Bottlebrush Polymers. *Soft Matter* **2019**, *15* (14), 2928–2941.

(16) Chremos, A.; Douglas, J. F. A Comparative Study of Thermodynamic, Conformational, and Structural Properties of Bottlebrush with Star and Ring Polymer Melts. *J. Chem. Phys.* **2018**, *149* (4), 044904.

(17) Kiani, C.; Chen, L.; Wu, Y. J.; Yee, A. J.; Yang, B. B. Structure and Function of Aggrecan. *Cell Res.* **2002**, *12* (1), 19–32.

(18) Seror, J.; Merkher, Y.; Kampf, N.; Collinson, L.; Day, A. J.; Maroudas, A.; Klein, J. Articular Cartilage Proteoglycans as Boundary Lubricants: Structure and Frictional Interaction of Surface-Attached Hyaluronan and Hyaluronan--Aggrecan Complexes. *Biomacromolecules* **2011**, *12* (10), 3432–3443.

(19) Chang, A. B.; Lin, T.-P.; Thompson, N. B.; Luo, S.-X.; Liberman-Martin, A. L.; Chen, H.-Y.; Lee, B.; Grubbs, R. H. Design, Synthesis, and Self-Assembly of Polymers with Tailored Graft Distributions. *J. Am. Chem. Soc.* **2017**, *139* (48), 17683–17693.

(20) van Genabeek, B.; de Waal, B. F. M.; Ligt, B.; Palmans, A. R. A.; Meijer, E. W. Dispersity under Scrutiny: Phase Behavior Differences between Disperse and Discrete Low Molecular Weight Block Co-Oligomers. *ACS Macro Lett.* **2017**, *6* (7), 674–678.

(21) Das, A.; Petkau-Milroy, K.; Klerks, G.; van Genabeek, B.; Lafleur, R. P. M.; Palmans, A. R. A.; Meijer, E. W. Consequences of Dispersity on the Self-Assembly of ABA-Type Amphiphilic Block Co-Oligomers. *ACS Macro Lett.* **2018**, *7* (5), 546–550.

(22) Lawrence, J.; Lee, S.-H.; Abdilla, A.; Nothling, M. D.; Ren, J. M.; Knight, A. S.; Fleischmann, C.; Li, Y.; Abrams, A. S.; Schmidt, B. V. K. J.; Hawker, M. C.; Connal, L. A.; McGrath, A. J.; Clark, P. G.; Gutekunst, W. R.; Hawker, C. J. A Versatile and Scalable Strategy to Discrete Oligomers. *J. Am. Chem. Soc.* **2016**, *138* (19), 6306–6310.

(23) Takizawa, K.; Tang, C.; Hawker, C. J. Molecularly Defined Caprolactone Oligomers and Polymers: Synthesis and Characterization. *J. Am. Chem. Soc.* **2008**, *130* (5), 1718–1726.

(24) Ren, J. M.; Lawrence, J.; Knight, A. S.; Abdilla, A.; Zerdan, R. B.; Levi, A. E.; Oschmann, B.; Gutekunst, W. R.; Lee, S.-H.; Li, Y.; McGrath, A. J.; Bates, C. M.; Qiao, G. G.; Hawker, C. J. Controlled Formation and Binding Selectivity of Discrete Oligo(methyl Methacrylate) Stereocomplexes. *J. Am. Chem. Soc.* **2018**, *140* (5), 1945–1951.

(25) Oschmann, B.; Lawrence, J.; Schulze, M. W. Effects of Tailored Dispersity on the Self-Assembly of Dimethylsiloxane–Methyl Methacrylate Block Co-Oligomers. *ACS Macro Lett.* **2017**.

(26) Zhang, C.; Kim, D. S.; Lawrence, J.; Hawker, C. J. Elucidating the Impact of Molecular Structure on the 19F NMR Dynamics and MRI Performance of Fluorinated Oligomers. *ACS Macro Lett.* **2018**.

(27) Lawrence, J.; Goto, E.; Ren, J. M.; McDearmon, B.; Kim, D. S.; Ochiai, Y.; Clark, P. G.; Laitar, D.; Higashihara, T.; Hawker, C. J. A Versatile and Efficient Strategy to Discrete Conjugated Oligomers. *J. Am. Chem. Soc.* **2017**, *139* (39), 13735–13739.

(28) Ogbonna, N. D.; Dearman, M.; Bharti, B.; Peters, A. J.; Lawrence, J. Elucidating the Impact of Side Chain Dispersity on the Assembly of Bottlebrush Polymers at the Air-water Interface. *J. Polym. Sci. A* **2021**, No. pol.20210565. https://doi.org/10.1002/pol.20210565.

(29) Nguyen, H. V.-T.; Jiang, Y.; Mohapatra, S.; Wang, W.; Barnes, J. C.; Oldenhuis, N. J.; Chen, K. K.; Axelrod, S.; Huang, Z.; Chen, Q.; Golder, M. R.; Young, K.; Suvlu, D.; Shen, Y.; Willard, A. P.; Hore, M. J. A.; Gómez-Bombarelli, R.; Johnson, J. A. Bottlebrush Polymers with Flexible Enantiomeric Side Chains Display Differential Biological Properties. *Nat. Chem.* **2021**. https://doi.org/10.1038/s41557-021-00826-8.

(30) Romio, M.; Grob, B.; Trachsel, L.; Mattarei, A.; Morgese, G.; Ramakrishna, S. N.; Niccolai, F.; Guazzelli, E.; Paradisi, C.; Martinelli, E.; Spencer, N. D.; Benetti, E. M. Dispersity within Brushes Plays a Major Role in Determining Their Interfacial Properties: The Case of Oligoxazoline-Based Graft Polymers. *J. Am. Chem. Soc.* **2021**. https://doi.org/10.1021/jacs.1c08383.

(31) Jha, S.; Dutta, S.; Bowden, N. B. Synthesis of Ultralarge Molecular Weight Bottlebrush Polymers Using Grubbs' Catalysts. *Macromolecules* **2004**, *37* (12), 4365–4374.

(32) Xia, Y.; Boydston, A. J.; Grubbs, R. H. Synthesis and Direct Imaging of Ultrahigh Molecular Weight Cyclic Brush Polymers. *Angewandte Chemie International Edition*. 2011, pp 5882–5885. https://doi.org/10.1002/anie.201101860.

(33) Li, Z.; Zhang, K.; Ma, J.; Cheng, C.; Wooley, K. L. Facile Syntheses of Cylindrical Molecular Brushes by a Sequential RAFT and ROMP "Grafting-through" Methodology. *J. Polym. Sci. A Polym. Chem.* **2009**, *47* (20), 5557–5563.

(34) Kim, K.; Seo, M. G.; Jung, J.; Ahn, J.; Chang, T.; Jeon, H. B.; Paik, H.-J. Direct Introduction of Hydroxyl Groups in Polystyrene Chain Ends Prepared by Atom-Transfer Radical Polymerization. *Polym. J.* **2019**, *52* (1), 57–64.

(35) Sanford, M. S.; Love, J. A.; Grubbs, R. H. A Versatile Precursor for the Synthesis of New Ruthenium Olefin Metathesis Catalysts. *Organometallics* **2001**, *20* (25), 5314–5318.

(36) Radzinski, S. C.; Foster, J. C.; Scannelli, S. J.; Weaver, J. R.; Arrington, K. J.; Matson, J. B. Tapered Bottlebrush Polymers: Cone-Shaped Nanostructures by Sequential Addition of Macromonomers. *ACS Macro Lett.* **2017**, *6* (10), 1175–1179.

(37) Lunn, D. J.; Seo, S.; Lee, S.-H.; Zerdan, R. B.; Mattson, K. M.; Treat, N. J.; McGrath, A. J.; Gutekunst, W. R.; Lawrence, J.; Abdilla, A.; Anastasaki, A.; Knight, A. S.; Schmidt, B. V. K. J.; Bates, M. W.; Clark, P. G.; DeRocher, J. P.; Van Dyk, A. K.; Hawker, C. J. Scalable Synthesis of an Architectural Library of Well-Defined Poly(acrylic Acid) Derivatives: Role of Structure on Dispersant Performance. *J. Polym. Sci. A Polym. Chem.* **2019**, *57* (6), 716–725.

(38) Whitfield, R.; Parkatzidis, K.; Rolland, M.; Truong, N. P.; Anastasaki, A. Tuning Dispersity by Photoinduced Atom Transfer Radical Polymerisation: Monomodal Distributions with Ppm Copper Concentration. *Angew. Chem. Int. Ed Engl.* **2019**, *58* (38), 13323–13328.

(39) Teo, Y. C.; Xia, Y. Importance of Macromonomer Quality in the Ring-Opening Metathesis Polymerization of Macromonomers. *Macromolecules* **2015**, *48* (16), 5656–5662.

(40) Sveinbjörnsson, B. R.; Weitekamp, R. A.; Miyake, G. M.; Xia, Y.; Atwater, H. A.; Grubbs, R. H. Rapid Self-Assembly of Brush Block Copolymers to Photonic Crystals. *Proc. Natl. Acad. Sci. U. S. A.* **2012**, *109* (36), 14332–14336.

(41) Walsh, D. J.; Lau, S. H.; Hyatt, M. G.; Guironnet, D. Kinetic Study of Living Ring-Opening Metathesis Polymerization with Third-Generation Grubbs Catalysts. *J. Am. Chem. Soc.* **2017**, *139* (39), 13644–13647.

(42) Ren, N.; Yu, C.; Zhu, X. Topological Effect on Macromonomer Polymerization. *Macromolecules* **2021**, *54* (13), 6101–6108.

(43) Radzinski, S. C.; Foster, J. C.; Chapleski, R. C., Jr; Troya, D.; Matson, J. B. Bottlebrush Polymer Synthesis by Ring-Opening Metathesis Polymerization: The Significance of the Anchor Group. *J. Am. Chem. Soc.* **2016**, *138* (22), 6998–7004.

(44) Flory, P. J. *Principles of Polymer Chemistry*; Cornell University Press, 1953.

(45) Zhao, L.; Byun, M.; Rzayev, J.; Lin, Z. Polystyrene–Polylactide Bottlebrush Block Copolymer at the Air/Water Interface. *Macromolecules* **2009**, *42* (22), 9027–9033.

(46) Burdyńska, J.; Daniel, W.; Li, Y.; Robertson, B.; Sheiko, S. S.; Matyjaszewski, K. Molecular Bottlebrushes with Bimodal Length Distribution of Side Chains. *Macromolecules* **2015**, *48* (14), 4813–4822.

(47) Sheiko, S. S.; Zhou, J.; Arnold, J.; Neugebauer, D.; Matyjaszewski, K.; Tsitsilianis, C.; Tsukruk, V. V.; Carrillo, J.-M. Y.; Dobrynin, A. V.; Rubinstein, M. Perfect Mixing of Immiscible Macromolecules at Fluid Interfaces. *Nat. Mater.* **2013**, *12* (8), 735–740.

(48) Lebedeva, N. V.; Nese, A.; Sun, F. C.; Matyjaszewski, K.; Sheiko, S. S. Anti-Arrhenius Cleavage of Covalent Bonds in Bottlebrush Macromolecules on Substrate. *Proc. Natl. Acad. Sci. U. S. A.* **2012**, *109* (24), 9276–9280.